Effects of Magnetic Abrasive Finishing on the Microstructure and Mechanical Properties of Inconel 718 Processed by Laser Powder Bed Fusion

Yunhao Zhao[a], Jason Ratay[b], Kun Li[a], Hitomi Yamaguchi[b*], Wei Xiong[a*]

a. Physical Metallurgy and Materials Design Laboratory, Department of Mechanical Engineering and Materials Science, University of Pittsburgh, Pittsburgh, PA 15261, USA
b. Department of Mechanical and Aerospace Engineering, University of Florida, Gainesville, FL 32611, USA

** Corresponding authors: Email: hitomiy@ufl.edu, weixiong@pitt.edu*

Abstract

Surface finishing is challenging for additively manufactured components with complex geometries. Magnetic abrasive finishing (MAF) is a promising surface finishing technology that can refine the surface quality of components with complex shapes produced by additive manufacturing. However, there is insufficient study regarding the impact of MAF on microstructure-property relationships for additively manufactured builds, which is critical for evaluating the mechanical performance. Furthermore, although MAF is usually used as the final step of post-processing, it remains unclear whether adjusting the sequence between MAF and other processes, e.g., heat treatment, can potentially improve the mechanical performance. In this work, the effects of MAF on the microstructure and mechanical property evolution of Inconel 718 superalloys made by laser powder bed fusion (LPBF) were studied. The application of MAF was found to significantly reduce the surface roughness of alloys and refine the grain size of aged samples. Moreover, MAF is able to increase the elongation of materials, which can be further influenced by the sequence of MAF and different heat treatments. The highest elongation can be achieved when MAF is performed between homogenization and aging processes. This work demonstrated a promising solution to improving the performance of LPBF Inconel 718 by combining MAF and heat treatment, which provides new perspectives on the post-processing development of additively manufactured alloys for advanced mechanical properties.

Keywords: Magnetic abrasive finishing; microstructure evolution; mechanical property; laser powder bed fusion; Inconel 718

 doi:10.20944/preprints202202.0253.v1

1. Introduction

Additive manufacturing is considered as a promising solution to fabricating structural metallic components requiring complex geometries and high precision. Meanwhile, the additively building strategy can reduce the waste of materials when compared with the traditionally subtractive manufacturing, such as computer numerical control (CNC) machining, which removes the materials from a bulk material. Though the revolutionary merits brought by additive manufacturing, there are still some issues accompanied during the manufacturing process. One of the major problems is the high surface roughness of the materials processed by additive manufacturing, which can deteriorate the material performance [1–4]. Therefore, surface finishing technologies are necessary for additively manufactured components to improve the mechanical properties [5,6].

Magnetic abrasive finishing (MAF) technology has been developed for several decades for finishing surface of workpieces with complex structures. The surface finishing is achieved by the relative motion between the workpiece and the magnetic abrasive, which is a mixture of magnetic particles and abrasive particles [7]. The unique processing features make it to have prominent advantages. First, it was found to effectively reduce surface roughness to a range of 0.01~1 μm and to improve surface wear resistance [8,9]. Second, it can polish workpieces with uneven surfaces, such as straight or bent tubes [10]. Third, it can finish the internal surface of workpieces. Yamaguchi et al. [11,12] developed an internal MAF process for polishing internal surface of components, and they applied it to the surface finishing of bent tubes made by Alumina ceramics and SUS304 stainless steels, demonstrating the potential of the wide application of MAF on various types of materials. They achieved a surface roughness of 0.02 μm for Alumina ceramic tubes and 0.03-0.04 μm for SUS303 stainless steels with negligible additional residual stress introduced to the surface. Moreover, the MAF technology can avoid chemical contamination compared with other surface finishing methods such like chemical- or electro-polishing [13].

Because the surfaces of additively manufactured components are usually freeform and intricate [13], the MAF technology can be a promising solution to improving the surface quality. Multiple studies applying MAF on additively manufactured alloys have been reported. Yamaguchi et al. [6] reduced the surface roughness Rz of 316L stainless steels

 doi:10.20944/preprints202202.0253.v1

made by selective laser melting (SLM) to 0.1 μm with the initial value over 100 μm. An integrated polishing strategy was used by combining sanding, magnetic field-assisted polishing (MAP), and magnetic field-assisted burnishing (MAB). The authors found both the MAP and MAB methods can introduce compressive stress on the workpiece surface, whereas the compressive stress magnitude imparted by MAB is much more than that by MAP and is able to transfer the surface stress from tensile to compressive. In another work of Wu and Yamaguchi [14], the authors investigated the influence of abrasive particle size and type (i.e., either magnetic or conventional) on the mechanisms of mechanical removal of materials and the resulted surface properties of SLM 316L stainless steel workpieces. It was concluded that the finishing using magnetic abrasive particles can effectively refine the surface with controlled material removal rate in contrast with the traditional abrasive. The large abrasive particles mainly contribute to removing materials from the peaks of the surface geometry, whereas the small abrasive particles can remove materials along the target surface features. Zhang et al. [13] investigated the MAF process on SLM 316L stainless steels components with different slope angles that representing the shape effects of workpiece on the finishing process. The MAF process was determined to effectively remove the defects such as partially bonded particles and balling features and to reduce the surface roughness Rz with a maximum level of 75.7%. Substantial mechanical work was required within a considerable volume to achieve a successful polishing process. Teng et al. [15] polished SLM AlSi10Mg alloy by combining grinding process and MAF process and achieved the finest surface roughness up to 0.155 μm. In addition, they concluded the MAF can reduce the surface hardness by removing the shallow work-hardened materials and release internal energy, whereas a long-time MAF process can keep the hardness values stable.

Inconel 718 Ni-based superalloy has been widely used in aerospace industries due to good high-temperature mechanical performance and corrosion resistance [16–18], and is popular among the additive manufacturing communities due to its good printability [19]. Using MAF technology for surface finishing of Inconel 718 alloy has attracted interests from researchers. For example, Choudhary et al. [20] and Singh et al. [21] reported successful surface finishing of the Inconel 718 alloys using MAF with the final surface roughness between 0.046 to 0.254 μm. The processing time, pole rotational speed, and

Preprints (www.preprints.org) | NOT PEER-REVIEWED | Posted: 21 February 2022 doi:10.20944/preprints202202.0253.v1

constituent of abrasive particles are found to be the major factors that affect the finishing results. Kumar and Singh [22] investigated the chemically assisted MAF process on Inconel 718 workpieces. The chemical solution was reported to promote the finishing process, but the effectiveness of the chemical solution with a certain concentration will also depend on the processing time and constituent of abrasive particles. In another research conducted by Chaurasia and Wankhede [23], the effects of process parameters of MAF on the surface roughness evolution of Inconel 718 was studied. The parameters optimized by [23] resulted in a surface roughness reduction of 87.1% compared to the initial condition and an Ra of 0.316 μm was obtained. The working gap between magnet pole and workpiece was found to contribute the most to the surface finishing.

Despite the reported work with respect to the application of MAF on Inconel 718 alloys, however, few research was done in terms of the using MAF on Inconel 718 alloys processed by additive manufacturing. Meanwhile, while most of the reported work only focused on the MAF process parameter optimization or on the impact of MAF process on the surface structure and roughness evolution, whether the MAF can also impact the interior microstructure and can further impact the mechanical properties of materials remains unknown, especially for additively manufactured Inconel 718 alloys. Additionally, it is intriguing to reveal whether MAF process can cause different effects when being applied together with heat treatment, which is an indispensable step of post-processing for additively manufactured Inconel 718 alloys [24–26]. Consequently, the present work aims to study the MAF process influence on the microstructure and property evolution in additively manufactured Inconel 718. In this work, Inconel 718 components processed by laser powder bed fusion (LPBF) were subject to various sequences of heat treatment and MAF process, and the microstructures resulted from different post-processing were characterized to determine the impact from MAF and heat treatment. Tensile testing was conducted to investigate the post-processing effects on mechanical performance. The process-structure-property relationships of LPBF Inconel 718 related to MAF process were revealed and the explanations to the underlying mechanisms were made.

Preprints (www.preprints.org) | NOT PEER-REVIEWED | Posted: 21 February 2022 doi:10.20944/preprints202202.0253.v1

2. Experiments

The Inconel 718 alloys used in this work were built via LPBF method by an EOS M 290 3D-printer (EOS company). The Inconel 718 powder was produced by Praxair, Inc. with a composition of Ni-18.26Fe-18.87Cr-4.97Nb-2.97Mo-0.94Ti-0.46Al-0.03C-0.06Mn-0.23Co-0.05Cu-0.06Si, in wt.%. The nominal powder sizes of d_{10}, d_{50}, and d_{90} were 18.5, 20, and 44 μm, respectively. The printing parameters were the default values implemented in the 3D-printer and were specifically designed for Inconel 718 alloys by the vendor, from which the laser power was 285 W, the scan velocity was 960 mm/s, and the hatching space between two neighboring scan tracks was 0.11 mm. The travel directions of the laser of two adjacent layers have a rotate angle of 67°. The alloys were built as tensile bars with a dog-bone geometry according to the ASTM E8/E8M-16a standard [27]. The dimensions of the tensile bars can be found in Table 1. All the tensile bars were built horizontally with the long axis perpendicular to the build direction. The tensile bars were then subject to various post-processing conditions with different heat treatments and MAF processes. The sample/processing notations with corresponding processing conditions are summarized in Table 2. The homogenization process of 1180°C-1h is named as "H", the aging process of 718°C-15h+650°C-10h is named as "A", and the MAF process is noted as "MAF" in the notations. The heat treatment was optimized from one of the authors' unpublished works. When being heat-treated, the tensile bars were encapsulated into quartz tubes with a back-filled Ar atmosphere for oxidation resistance and were then quenched into ice-water when the heat treatment was done. Figure 1 shows a schematic of the MAF finishing principle for flat Inconel 718 workpieces. A mixture of magnetic particles and abrasive is magnetized in the magnetic field, forms a particle brush along the lines of the magnetic field, and presses against the workpiece due to the magnetic force. When the magnet is rotated and translated, the particle brush is dragged by the magnet while conforming to the target surface. The relative motion of the particle brush against the target surface removes material and smooths the target surface.

An experimental setup (Fig. 2) was created, using a 5-axis CNC machining center, based on the processing principle. Table 1 shows the experimental conditions. A mixture of 0.9 g of G25 steel grit and 0.1 g of 126 μm friable wheel grit, uncoated diamond abrasive

Preprints (www.preprints.org) | NOT PEER-REVIEWED | Posted: 21 February 2022 doi:10.20944/preprints202202.0253.v1

(which enables more effective material removal than coated abrasive [28]) was used in the experiments with a set of Nd-Fe-B magnets (a ∅12.7×12.7 mm magnet centered on three ∅25.4×12.7 mm magnets). Under the specified experimental conditions, the magnetic force acting on the target surface (normal to the target surface) measured 2 N. The finishing pressure at the middle of the 6-mm-wide workpiece was therefore estimated to be 26.2 kPa. The linear path of the magnet began at the edge of the workpiece. The magnet was fed 330 times for a stroke of 80 mm at a feed rate of 1 mm/s. After finishing, the workpiece was rinsed with ethanol in an ultrasonic cleaner for further evaluation.

The surface roughness (Ra and Rz) of the workpiece surface was measured using a stylus surface roughness tester (Mitutoyo Surftest SJ-400) before and after finishing to determine the effects of MAF on the surface quality. The roughness measurement points are shown in Fig. 3. Since the samples were built horizontally, there were two different surfaces when the tensile bars were sectioned using an electric discharge machining (EDM) machine from the substrate, i.e., one printed surface and one EDM-cut surface. For roughness measurement, scans with a length of 4 mm were conducted on both printed and EDM-cut surfaces of each sample, as shown by red arrows in Fig. 3, and the average values of the scans were calculated and used to represent the surface roughness on the particular surface.

The tensile tests were performed on an MTS Landmark Servohydraulic Test System using a strain rate of 1 mm/min. The fractography of the samples were characterized by a ZEISS-Sigma 500 VP SEM. The EBSD (FEI Scios Dual-Beam system) characterization was performed on samples cut from the grip parts of the tensile bars after tensile testing to investigate the effects of MAF on the microstructure and to exclude the impact from the deformation caused by the externally applied tension. In addition, it should be noted that the selection of samples cut for EBSD characterization also ruled out the regions that may be affected by the grip indents resulted from the tensile testing. A scan area of 3000 x 3000 μm and a step size of 5 μm were adopted for the EBSD mapping. The longitudinal planes parallel to the build direction were characterized.

Preprints (www.preprints.org) | NOT PEER-REVIEWED | Posted: 21 February 2022 doi:10.20944/preprints202202.0253.v1

3. Results

3.1. Surface roughness after MAF

The MAF process was found to effectively improve surface quality and to significantly reduce the surface roughness of the heat-treated samples. The surface roughness of samples H+A and H+A+MAF were characterized as examples for surface quality analysis in this work. As can be seen from Fig. 3, both the printed (Fig. 3(b)) and EDM-cut (Fig. 3(d)) surfaces become shining after MAF process, whereas before being processed by MAF (Figs. 3(a)&(c)) the oxides formed on the surface during water quenching or EDM cutting made the surfaces luster-lacking. Table 3 compares the Ra and Rz values at different locations on each surface before and after MAF process. It can be found that the Ra and Rz at different locations on both surfaces decrease remarkably with the MAF process applied. More specifically, on the printed surface finished by MAF, the average Ra is reduced from 2.0 μm to 0.46 μm and the Rz decreases from 11.0 μm to 2.47 μm, respectively. Similarly, on the EDM-cut surface processed by MAF, both the average Ra and Rz values decrease vastly (from 3.55 μm to 0.15 μm for Ra; and from 21.3 μm to 1.3 μm for Rz). The roughness measurement results show that the MAF process can reduce the surface roughness for both types of surfaces of LPBF alloys. The reduced values of Rz achieved after MAF indicate that the process can improve the surface roughness uniformity by reducing the maximum height differences between the surface peaks and valleys. It should be noted that although the average values of Ra (2.0 μm) and Rz (11.0 μm) of the printed surface are lower than that of the EDM-cut surface (Ra: 3.55 μm, Rz: 21.3 μm) before the application of MAF, they become higher (Ra: 0.46 μm and Rz: 2.47 of the printed surface) than their counterparts (Ra: 0.15 μm and Rz: 1.3 μm of the EDM-cut surface) after being processed by MAF. This is because the printed surface is uneven as the surface was cyclically melted and printing textures were formed during the LPBF process.

3.2. Microstructure evolution

Figure 4 compares the effects of MAF and heat treatment on the microstructure evolution in LPBF Inconel 718 alloys. The grain size evolution is demonstrated by inverse pole figures (IPFs), as shown in Figs. 4(a1)-(e1), and the average area-weighted [25] grain

Preprints (www.preprints.org) | NOT PEER-REVIEWED | Posted: 21 February 2022 doi:10.20944/preprints202202.0253.v1

sizes of each sample were obtained from the EBSD characterization and are listed in Fig. 4. Kernel average misorientation (KAM) values of each sample generated from EBSD are used to signify the change of internal strain levels [29] with different processes. The KAM values at each measured point are the average misorientation angles between the measured points and their surrounding neighbors [30]. The neighboring points within the 3rd kernel outside each measured points were counted in this work for the KAM calculation. A higher KAM level within one sample indicates it is associated with a higher level of geometrically necessary dislocations [30], and thus implies a higher internal strain level. Because the KAM mainly reflects the localized strain level within one sample, the average KAM value is not adopted in this work for microstructure analysis; alternatively, the KAM maps are given in Figs. 4(a2)-(e2) to illustrate the local strain distribution. Moreover, grain boundary maps obtained from EBSD are presented in Figs. 4(a3)-(e3), the grain boundary density (GBD) is used to evaluate the grain boundary evolution with respect to the MAF and heat treatment conditions [24] and the GBD values are shown in Fig. 4.

The comparison between samples H and H+MAF (Figs. 4(a1)&(b1)) indicates that the average grain size of the homogenized sample H is not changed after processed by MAF. Accordingly, the GBD values of samples H and H+MAF are comparable (Figs. 4(a3)&(b3)). However, the local strain level increases with the application of MAF, as shown in Figs. 4(a2)&(b2). For the homogenized sample H, the KAM level after aging in sample H+A is found to be comparable or slightly lower than its counterpart before aging, implying the aging treatment does not introduce extra strain into the homogenized alloy. The subsequent aging process after homogenization can increase the grain size from 259 μm to 294.7 μm, as displayed by Figs. 4(a1)&(c1), and the GBD value is reduced (Figs. 4(a3)&(c3)). On the contrary, the grain size is reduced after aging when the homogenized sample is treated with MAF, as shown in the comparison between samples H+MAF (Fig. 4(b1)) and H+MAF+A (Fig. 4(e1)), of which the grain size values are 261.3 μm and 225.4 μm, respectively. Such an observation indicates the introduction of aging after MAF process can lead to grain refinement in the LPBF Inconel 718 alloys. In addition, the aging step after MAF can also help with reducing the internal strain, which can be found from the reduced KAM level of sample H+MAF+A (Fig. 4(e2)) with respect to that in sample

Preprints (www.preprints.org) | NOT PEER-REVIEWED | Posted: 21 February 2022 doi:10.20944/preprints202202.0253.v1

H+MAF (Fig. 4(b2)). Nevertheless, subsequent aging process after homogenization without the MAF process does not significantly change the KAM level (Figs. 4(a2)&(c2)).

For the aged samples which are illustrated by Figs. 4(c1)&(d1), the application of MAF is found to refine grain size from 294.7 μm of the sample H+A to 234.4 μm of the sample H+A+MAF. Figures 4(c2)&(d2) show a slight increase in KAM level is caused due to MAF process. Moreover, because the MAF conducted right after homogenization (sample H+MAF as shown in Fig. 4(b1)) cannot change the grain size compared to that of the homogenized sample H (Fig. 4(a1)), it can be concluded that the grain refinement can be achieved when the MAF is performed following the aging process rather than the homogenization process. Besides, the comparisons of KAM levels between samples H (Fig. 4(a2)) and H+MAF (Fig. 4(b2)), and between samples H+A (Fig. 4(c2)) and H+A+MAF (Fig. 4(d2)) all indicate an increase of KAM inside of samples due to MAF process, which indicate the MAF process can introduce strain into samples regardless the preliminary heat treatment conditions.

A further inspection into the grain boundary shows that the high angle grain boundaries is predominant in all samples, as illustrated in Figs. 4(a3)-(e3). However, the low angle grain boundary fractions of each sample are close to 2%. Hence, the influence of the low angle grain boundary can be negligible. The increase in the GBD of sample H+A+MAF (Fig. 4(d3)) compared with that of sample H+A (Fig. 4(c3)) indicates the MAF process mainly introduces high angle grain boundaries. Similar conclusions can be made by comparing samples H+MAF (Fig. 4(b3)) and H+MAF+A (Fig. 4(e3)), from which the aging process following MAF process increases high angle grain boundaries.

3.3. Tensile properties and fractography

Tensile properties and fractography characterizations were performed on samples H+A, H+A+MAF, and H+MAF+A to investigate the processing influence on the alloys. The engineering stress-strain properties of alloys with various processes shown in Fig. 5 and Table 4 indicate that the MAF process performed after aging (sample H+A+MAF) can achieve the highest yield strength of 1152.1 MPa and highest ultimate tensile strength up to 1340.4 MPa, which are slightly beyond the sample H+A without MAF process. Furthermore, the elongation has been significantly improved from 14% of sample H+A to

Preprints (www.preprints.org) | NOT PEER-REVIEWED | Posted: 21 February 2022 doi:10.20944/preprints202202.0253.v1

19.8% of sample H+A+MAF with the application of MAF. When the MAF is performed between homogenization and aging processes, i.e., for sample H+MAF+A, the yield strength and ultimate tensile strength are between that of samples H+A and H+A+MAF. However, the highest elongation is achieved in sample H+MAF+A, which is up to 22.7% according to Table 4. The tensile testing results indicate that the MAF process can significantly improve the elongation properties of heat-treated LPBF Inconel 718 alloys and meanwhile slightly refine their strength properties. The MAF performed between homogenization and aging is found to result in the highest elongation, whereas the MAF performed after aging can achieve the highest strength among the alloys.

The fractography of the tensile samples displayed in Fig. 6 shows ductile fracture features in all the three samples. The fractography of each sample is consisted of a shear slip region near the surface and a fibrous region inside of the sample. The shear slip region and fibrous region are divided by a notable boundary depicted by white dashed lines in Figs. 6(a), (c), and (e). The thickness of the shear slip regions in different samples are close. The radial region is not observed in the samples, indicating the alloys have good plasticity. Ductile dimples in the shear slip regions are shown in Figs. 6(b), (d), &(f), the shape and size of the dimples are comparable among the alloys. The fractography characterization implies the MAF process does not significantly influence the fracture mechanisms of LPBF Inconel 718.

4. Discussions

4.1. Effects of MAF and heat treatment on microstructure evolution

The influence of MAF on the microstructure evolution is mainly related to the grain refinement and dislocation density change as described in section 3.2. The refined grain size can be obtained in both samples H+A+MAF and H+MAF+A (Figs. 4(d1)&(e1)), which means the combination of aging and MAF processes can effectively refine grains. On the contrary, performing only MAF process on the homogenized sample does not change grain size, as shown in Fig. 4(b1), and the aging process without MAF can lead to coarse grains (Fig. 4(c1)). The increase in KAM levels after MAF indicates such a process can introduce external energy and dislocations into the materials. Dislocation density

 doi:10.20944/preprints202202.0253.v1

change reflected by the KAM level can be increased with the introduction of MAF. Such effects can be observed in both homogenized sample H+MAF (Fig. 4(b2)) and aged sample H+A+MAF (Fig. 4(d2)), but the aging following MAF process can instead reduce the dislocation density, as shown in Figs. 4(b2)&(e2). Without the application of MAF, the aging can cause negligible change on the dislocation density (Fig. 4(c2)).

Although grain refinement is achieved in both samples H+A+MAF and H+MAF+A, the mechanisms of the refinement for the two samples can be different. For sample H+A+MAF, the MAF process introduced after aging can be concluded to break existing grain boundaries obtained after aging (i.e., sample H+A) and hence form new grain boundaries. Details of such a mechanism remains to be further studied. However, a reasonable explanation can be made, that the process is realized by the direct interaction of γ″ strengthening precipitates that are largely formed during the aging process with the energy introduced during the MAF process. Since few low angle grain boundaries are observed, it can be deduced that the high angle grain boundaries are directly formed during the MAF process. For sample H+MAF+A, the grain refinement should happen during the aging process because the grain size in sample H+MAF without aging remains at a high level. It can be assumed that the aging process after MAF can release the energy, which has been stored in the alloy reflected by high KAM level in sample H+MAF (Fig. 4(b2)). The energy release process further creates new grain boundaries in sample H+MAF+A by interacting with γ″ precipitates that being formed during aging. The grains are thus refined. In addition, since the high dislocation density in sample H+MAF is reduced after aging, it can be inferred that the dislocations further interact and contribute to form new grain boundaries.

4.2. Effects of MAF on tensile properties

The low surface roughness achieved by MAF process contributes to the improvement of elongation property. The removal of the surface defects, such as partially bonded particles, balling features, and oxides caused by LPBF and EDM cutting processes improves the uniformity of the materials and reduce potential stress concentration for cracking initiation and propagation. Additionally, the good elongation property can also be linked with the grain size refinement achieved in aged samples with MAF. Liu et al. [31]

Preprints (www.preprints.org) | NOT PEER-REVIEWED | Posted: 21 February 2022 doi:10.20944/preprints202202.0253.v1

found that the decrease in grain size of fcc/bcc metals can result in the improvement of uniform elongation when the grain size is larger than ~200 μm. From Figs. 4(c1), (d1) and (e1), samples H+A+MAF and H+MAF+A processed with MAF have smaller grain size than that of sample H+A without MAF. Accordingly, Fig. 5 shows that the samples H+A+MAF and H+MAF+A have higher uniform elongation than sample H+A, which agrees with the conclusions made by Liu et al. [31]. Therefore, it can be concluded that the improvement of elongation in samples processed with MAF comes from the grain refinement effect. A further investigation into the MAF processed samples indicates that the sample H+MAF+A has a slightly higher uniform elongation than that in sample H+A+MAF by an increment of ~1.4%, as can be seen in Fig. 5, which can be attributed to the smaller grain size of sample H+MAF+A (225.4 μm) than sample H+A+MAF (234.3 μm). The total elongation of sample H+MAF+A (22.7%) is higher than sample H+A+MAF (19.8%) with an increase of 2.9%, which is larger than the difference between the uniform elongation values of these two samples. Thus, a further increase in elongation occurs after necking in sample H+MAF+A compared to sample H+A+MAF. Such a phenomenon may be explained by the lower stress/strain level inside of the sample H+MAF+A (Fig. 4(e2)). However, a more specific study can be further conducted to determine the underlying mechanisms. Moreover, whether the MAF process can further influence the phase transformations during heat treatment and impact the mechanical properties accordingly remains a question and should thus attract more investigations.

Conclusions

- The MAF process can effectively reduce the surface roughness of as-built and heat-treated Inconel 718 alloys made by LPBF. Both the printed surface produced by LPBF and EDM surface generated from cutting can be significantly smoothed with the application of MAF.
- The combination of MAF and heat treatment can significantly influence the microstructure and property evolution of LPBF Inconel 718 alloys. The MAF process can increase internal strain in the alloys, but a subsequent aging process can mitigate the strain level. MAF process applied together with the aging process can reduce the

grain size and increase the grain boundary density of alloy. Such microstructure change can significantly improve the elongation property of the LPBF Inconel 718.

- The process sequence between MAF and heat treatment is found to affect the microstructure and further influence the elongation property. MAF applied between homogenization and aging can result in the highest elongation. However, materials strength is only slightly improved with the application of the MAF process.
- Introducing the MAF process can be a way for further microstructure refinement and property improvement for LPBF Inconel 718. An optimized process by coupling MAF and heat treatment is a promising post-processing strategy for additively manufactured alloys with improved performance.

Acknowledgements

The authors thank Swanson School of Engineering, University of Pittsburgh for the research support.

CRediT author statement

Yunhao Zhao: Validation, Formal analysis, Investigation (sample preparation, microstructure characterization and analysis), Data Curation, Writing - Original Draft; Jason Ratay: Validation, Investigation (sample preparation, microstructure analysis), Writing - Review & Editing; Kun Li: Investigation (sample preparation, mechanical testing); Hitomi Yamaguchi: Conceptualization, Methodology, Investigation, Writing - Review & Editing, Supervision, Project administration. Wei Xiong: Conceptualization, Methodology, Investigation, Writing - Review & Editing, Supervision, Project administration.

Notes for preprint

This work was initiated through the discussion between Wei Xiong and Hitomi Yamaguchi in 2019. Both Xiong and Yamaguchi designed the experiments together. Jason Ratay in Yamaguchi's lab performed the sample finishing. Kun Li in Xiong's lab initially handled microstructure characterization and mechanical property evaluation during his postdoc research studies. After Kun Li completed the postdoc research with Wei Xiong in Aug.

2020, Yunhao Zhao took over the tasks to wrap up the experiments. However, Yunhao Zhao observed some serious issues of microstructure analysis in the previous efforts, especially EBSD. Therefore, under the supervision of Wei Xiong and Hitomi Yamaguchi, Yunhao Zhao prepared new samples and re-performed microstructure analysis to conclude the work with manuscript preparation.

References

[1] H. Masuo, Y. Tanaka, S. Morokoshi, H. Yagura, T. Uchida, Y. Yamamoto, Y. Murakami, Influence of defects, surface roughness and HIP on the fatigue strength of Ti-6Al-4V manufactured by additive manufacturing, Int. J. Fatigue. 117 (2018) 163–179. https://doi.org/10.1016/j.ijfatigue.2018.07.020.

[2] K. Moussaoui, W. Rubio, M. Mousseigne, T. Sultan, F. Rezai, Effects of Selective Laser Melting additive manufacturing parameters of Inconel 718 on porosity, microstructure and mechanical properties, Mater. Sci. Eng. A. 735 (2018) 182–190. https://doi.org/10.1016/j.msea.2018.08.037.

[3] M. Balbaa, S. Mekhiel, M. Elbestawi, J. McIsaac, On selective laser melting of Inconel 718: Densification, surface roughness, and residual stresses, Mater. Des. 193 (2020) 108818. https://doi.org/10.1016/j.matdes.2020.108818.

[4] K.S. Chan, M. Koike, R.L. Mason, T. Okabe, Fatigue life of titanium alloys fabricated by additive layer manufacturing techniques for dental implants, Metall. Mater. Trans. A Phys. Metall. Mater. Sci. 44 (2013) 1010–1022. https://doi.org/10.1007/s11661-012-1470-4.

[5] Y. Kaynak, O. Kitay, The effect of post-processing operations on surface characteristics of 316L stainless steel produced by selective laser melting, Addit. Manuf. 26 (2019) 84–93. https://doi.org/10.1016/j.addma.2018.12.021.

[6] H. Yamaguchi, O. Fergani, P.Y. Wu, Modification using magnetic field-assisted finishing of the surface roughness and residual stress of additively manufactured components, CIRP Ann. - Manuf. Technol. 66 (2017) 305–308. https://doi.org/10.1016/j.cirp.2017.04.084.

[7] C. Qian, Z. Fan, Y. Tian, Y. Liu, J. Han, J. Wang, A review on magnetic abrasive finishing, Int. J. Adv. Manuf. Technol. 112 (2021) 619–634. https://doi.org/10.1007/s00170-020-06363-x.

[8] W. Li, X. Li, S. Yang, W. Li, A newly developed media for magnetic abrasive finishing process: Material removal behavior and finishing performance, J. Mater. Process. Technol. 260 (2018) 20–29. https://doi.org/10.1016/j.jmatprotec.2018.05.007.

[9] R.S. Mulik, P.M. Pandey, Magnetic abrasive finishing of hardened AISI 52100 steel, Int. J. Adv. Manuf. Technol. 55 (2011) 501–515. https://doi.org/10.1007/s00170-010-3102-8.

[10] M. Givi, A. Fadaei Tehrani, A. Mohammadi, Polishing of the aluminum sheets with magnetic abrasive finishing method, Int. J. Adv. Manuf. Technol. 61 (2012) 989–998. https://doi.org/10.1007/s00170-011-3753-0.

[11] H. Yamaguchi, T. Shinmura, Internal finishing process for alumina ceramic components by a magnetic field assisted finishing process, Precis. Eng. 28 (2004) 135–142. https://doi.org/10.1016/j.precisioneng.2003.07.001.

[12] H. Yamaguchi, T. Shinmura, M. Sekine, Uniform internal finishing of SUS304 stainless steel bent tube using a Magnetic abrasive finishing process, J. Manuf. Sci. Eng. Trans. ASME. 127 (2005) 605–611. https://doi.org/10.1115/1.1951786.

[13] J. Zhang, A. Chaudhari, H. Wang, Surface quality and material removal in magnetic abrasive finishing of selective laser melted 316L stainless steel, J. Manuf. Process. 45 (2019) 710–719. https://doi.org/10.1016/j.jmapro.2019.07.044.

[14] P.Y. Wu, H. Yamaguchi, Material Removal Mechanism of Additively Manufactured Components Finished using Magnetic Abrasive Finishing, Procedia Manuf. 26 (2018) 394–402. https://doi.org/10.1016/j.promfg.2018.07.047.

[15] X. Teng, G. Zhang, Y. Zhao, Y. Cui, L. Li, L. Jiang, Study on magnetic abrasive finishing of AlSi10Mg alloy prepared by selective laser melting, Int. J. Adv. Manuf. Technol. 105 (2019) 2513–2521. https://doi.org/10.1007/s00170-019-04485-5.

[16] M.M. Kirka, F. Medina, R. Dehoff, A. Okello, Mechanical behavior of post-processed Inconel 718 manufactured through the electron beam melting process, Mater. Sci. Eng. A. 680 (2017) 338–346. https://doi.org/10.1016/j.msea.2016.10.069.

[17] C.M. Kuo, Y.T. Yang, H.Y. Bor, C.N. Wei, C.C. Tai, Aging effects on the microstructure and creep behavior of Inconel 718 superalloy, Mater. Sci. Eng. A. 510–511 (2009) 289–294. https://doi.org/10.1016/j.msea.2008.04.097.

[18] A. Thomas, M. El-Wahabi, J.M. Cabrera, J.M. Prado, High temperature deformation of Inconel 718, J. Mater. Process. Technol. 177 (2006) 469–472. https://doi.org/10.1016/j.jmatprotec.2006.04.072.

[19] T. Trosch, J. Strößner, R. Völkl, U. Glatzel, Microstructure and mechanical properties of selective laser melted Inconel 718 compared to forging and casting, Mater. Lett. 164 (2016) 428–431. https://doi.org/10.1016/j.matlet.2015.10.136.

[20] A. Choudhary, H. Kumar, Studies in surface finishing of inconel718 flat surface with magnetic abrasive finishing, Int. J. Mech. Prod. Eng. Res. Dev. 7 (2017) 139–150. https://doi.org/10.24247/ijmperdaug201715.

[21] L. Singh, H. Kumar, A. Kumar, Parametric study in surface finishing of inconel 718 surface with magnetic abrasive finishing process, Int. J. Mech. Prod. Eng. Res. Dev. 7 (2017) 223–234. https://doi.org/10.24247/ijmperdaug201723.

[22] H. Kumar, G. Singh, Parametric studies on finishing of inconel 718 flat surfaces with chemically assisted magnetic abrasive finishing process, Mater. Today Proc. (2020). https://doi.org/10.1016/j.matpr.2020.09.110.

[23] A. Chaurasia, V. Wankhede, MAGNETIC ABRASIVE FINISHING OF INCONEL 718 SUPER ALLOY USING PERMANENT MAGNET Ankur, Int. Res. J. Eng.

Technol. 05 (2018) 1165–1168.

[24] Y. Zhao, F. Meng, C. Liu, S. Tan, W. Xiong, Impact of homogenization on microstructure-property relationships of inconel 718 alloy prepared by laser powder bed fusion, Mater. Sci. Eng. A. 826 (2021) 141973. https://doi.org/10.1016/j.msea.2021.141973.

[25] Y. Zhao, K. Li, M. Gargani, W. Xiong, A comparative analysis of Inconel 718 made by additive manufacturing and suction casting: Microstructure evolution in homogenization, Addit. Manuf. 36 (2020) 101404. https://doi.org/10.1016/j.addma.2020.101404.

[26] Y. Zhao, N. Sargent, K. Li, W. Xiong, A new high-throughput method using additive manufacturing for alloy design and heat treatment optimization, Materialia. 13 (2020) 1–5. https://doi.org/10.1016/j.mtla.2020.100835.

[27] ASTM International, E8/E8M−16a: Standard test methods for tension testing of metallic materials, ASTM Int. (2016). https://doi.org/10.1520/E0008_E0008M-16A.

[28] J. Ratay, P.-Y. Wu, A. Feirvezers, H. Yamaguchi, Characteristics of Diamond Abrasive Used in Magnetic Abrasive Finishing of Nickel-Based Superalloys, J. Micro-and Nano-Manufacturing. 8 (2020) 31007.

[29] J.S. Wang, C.C. Hsieh, C.M. Lin, E.C. Chen, C.W. Kuo, W. Wu, The effect of residual stress relaxation by the vibratory stress relief technique on the textures of grains in AA 6061 aluminum alloy, Mater. Sci. Eng. A. 605 (2014) 98–107. https://doi.org/10.1016/j.msea.2014.03.037.

[30] S. Sridar, Y. Zhao, W. Xiong, Cyclic re-austenitization of copper-bearing high-strength low-alloy steels fabricated by laser powder bed fusion, Mater. Charact. 166 (2020) 110437. https://doi.org/10.1016/j.matchar.2020.110437.

[31] H. Liu, Y. Shen, J. Ma, P. Zheng, L. Zhang, Grain Size Dependence of Uniform Elongation in Single-Phase FCC/BCC Metals, J. Mater. Eng. Perform. 25 (2016) 3599–3605. https://doi.org/10.1007/s11665-016-2245-7.

Preprints (www.preprints.org) | NOT PEER-REVIEWED | Posted: 21 February 2022 doi:10.20944/preprints202202.0253.v1

Tables

Table 1. MAF experimental conditions.

Workpiece	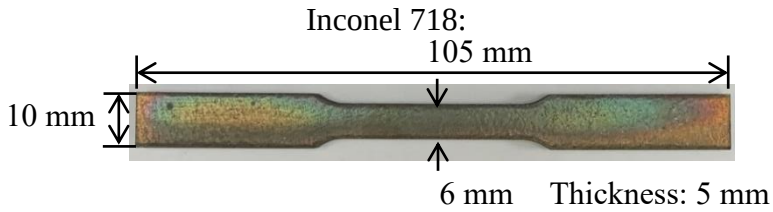
Magnetic particles	G25 steel grit: 0.9 g
Abrasive	126 μm mean diameter uncoated diamond abrasive: 0.1 g (additional 0.1 g added every 60 min)
Lubricant	Cutting fluid (Coolube® 2210EP): 0.4 mL (additional 0.05 mL every 2 min)
Magnet	Nd-Fe-B magnet: ∅25.4×12.7 mm (3), ∅12.7×12.7 mm (1)
Magnet revolution	600 min^{-1}
Magnet feed	80 mm at 1 mm/s
Clearance	2 mm
Polishing time	440 min (330 passes)

Table 2. The notations of sample and processing conditions.

Sample/processing notations	Processing Conditions
H	1180°C-1h
H+A	1180°C-1h+718°C-15h+650°C-10h
H+MAF	1180°C-1h+MAF
H+A+MAF	1180°C-1h+718°C-15h+650°C-10h+MAF
H+MAF+A	1180°C-1h+MAF+718°C-15h+650°C-10h

Preprints (www.preprints.org) | NOT PEER-REVIEWED | Posted: 21 February 2022 doi:10.20944/preprints202202.0253.v1

Table 3. Surface roughness measurement results (in μm) of the fully heat-treated samples before MAF process (H+A) and after MAF process (H+A+MAF).

Printed surface		Left	Middle	Right	Average
Before	Ra	1.53	1.76	2.7	2.0
	Rz	10.3	8.7	14.1	11.0
After	Ra	0.34	0.40	0.65	0.46
	Rz	2.1	2.4	2.9	2.47
EDM-cut surface		**Left**	**Middle**	**Right**	**Average**
Before	Ra	3.33	3.8	3.51	3.55
	Rz	19.7	21.4	22.7	21.3
After	Ra	0.14	0.15	0.15	0.15
	Rz	1.3	1.5	1.2	1.3

Table 4. Tensile properties of samples H+A, H+A+MAF, and H+MAF+A.

Sample	YS, MPa	UTS, MPa	Elongation, %
H+MAF+A	1148.6±1.8	1332.3±2.6	22.7±0.3
H+A+MAF	1152.1±1.5	1340.4±2.3	19.8±0.5
H+A	1142.8±2.1	1304±3.2	14.0±0.5

Preprints (www.preprints.org) | NOT PEER-REVIEWED | Posted: 21 February 2022 doi:10.20944/preprints202202.0253.v1

Figures

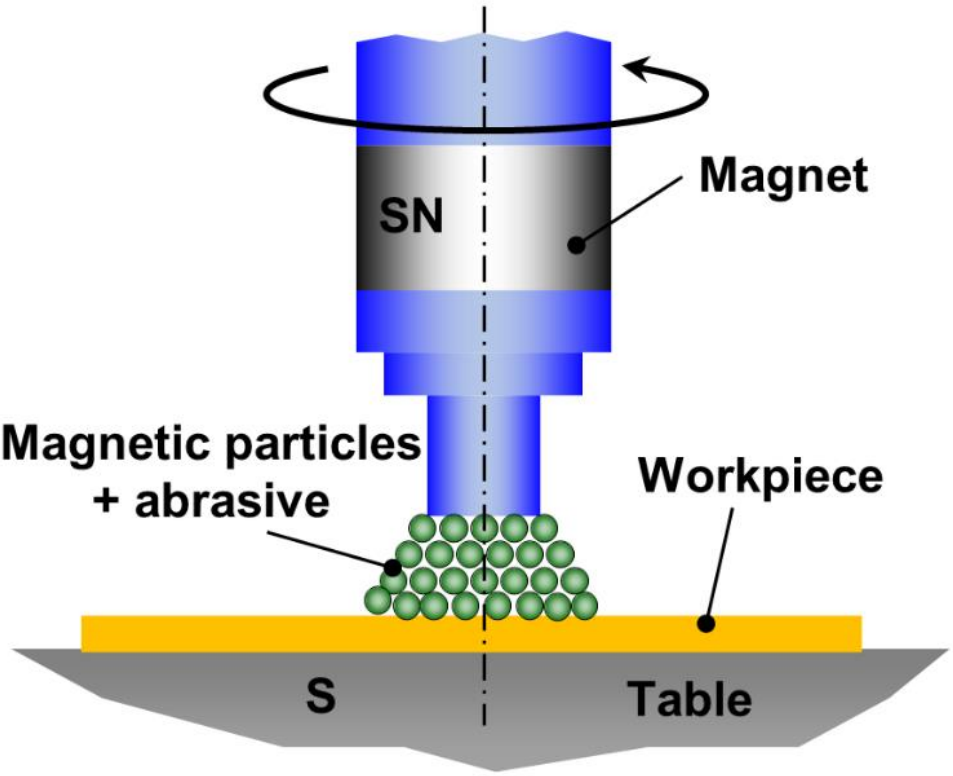

Figure 1. MAF processing principle.

Preprints (www.preprints.org) | NOT PEER-REVIEWED | Posted: 21 February 2022 doi:10.20944/preprints202202.0253.v1

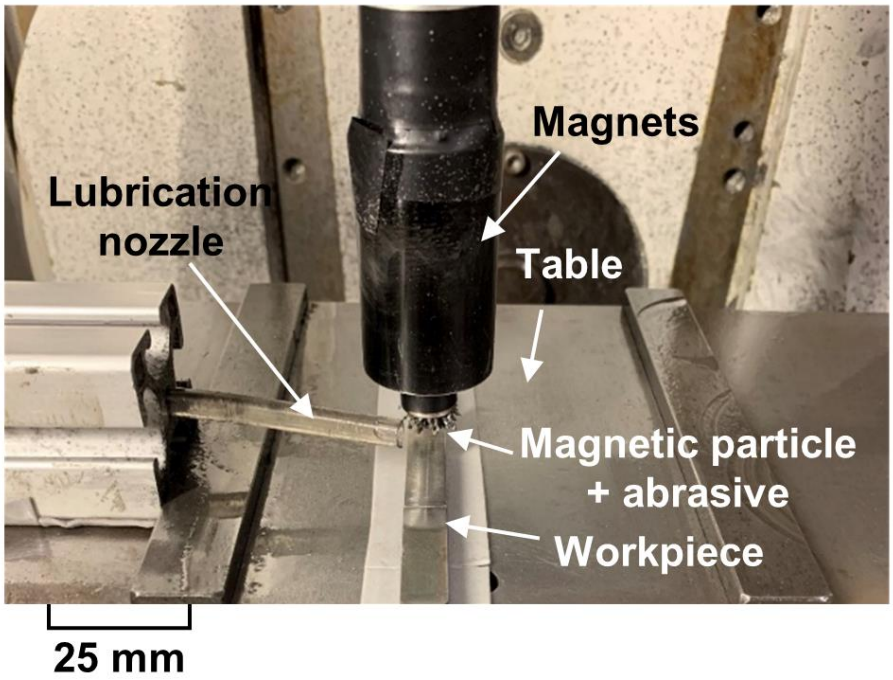

Figure 2. MAF polishing setup.

Preprints (www.preprints.org) | NOT PEER-REVIEWED | Posted: 21 February 2022 doi:10.20944/preprints202202.0253.v1

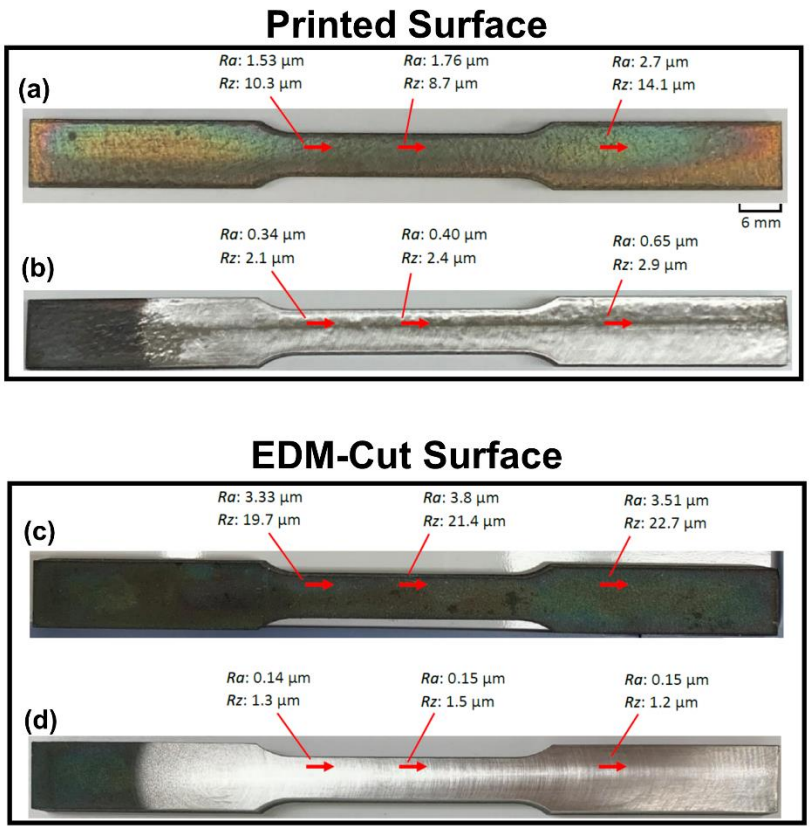

Figure 3. Images of the fully heat-treated samples before MAF process (H+A) and after MAF process (H+A+MAF): (a) printed surface before MAF and (b) after MAF; (c) EDM-cut surface before MAF and (d) after MAF.

Preprints (www.preprints.org) | NOT PEER-REVIEWED | Posted: 21 February 2022 doi:10.20944/preprints202202.0253.v1

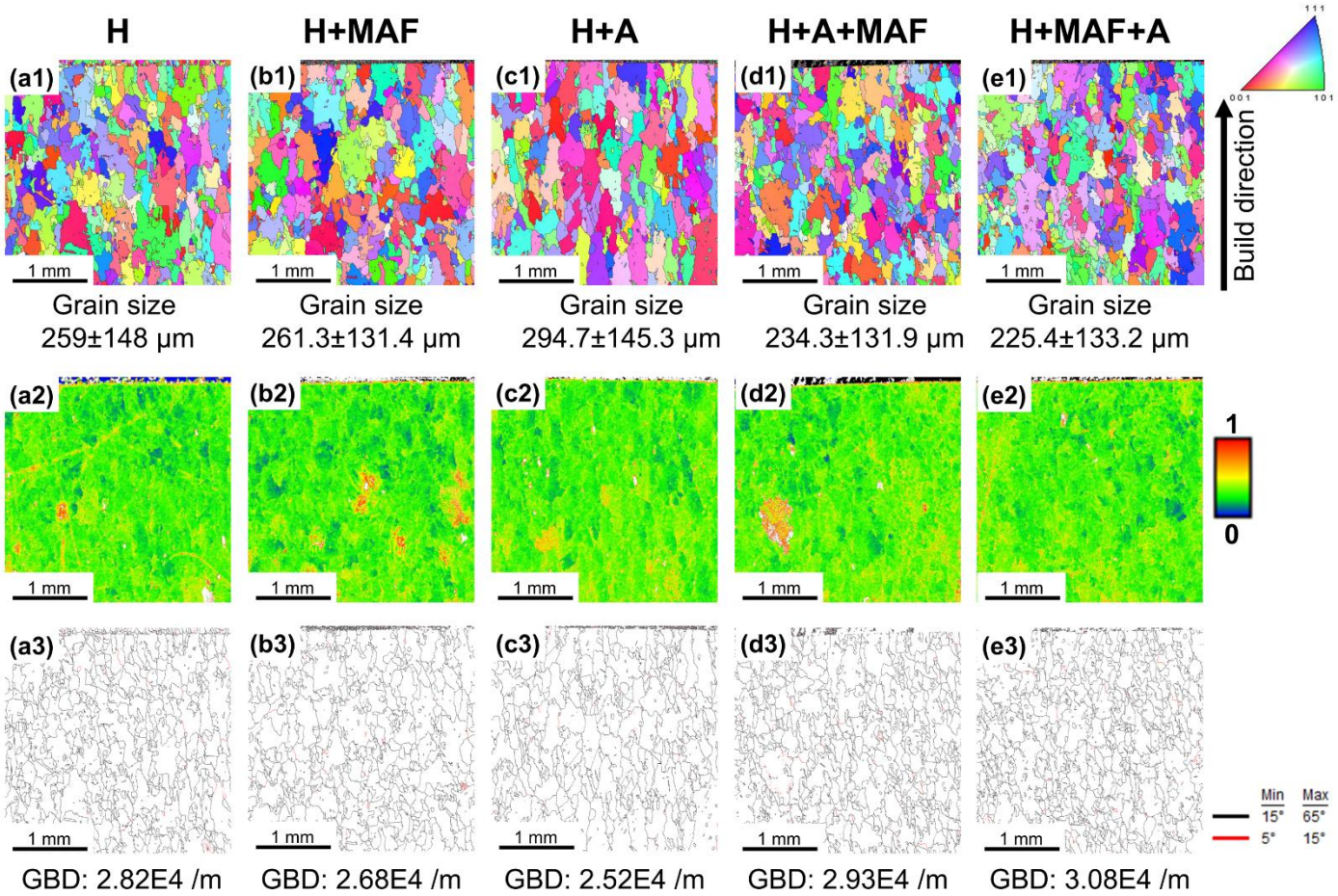

Figure 4. Microstructures analysis using EBSD maps of Inverse Pole Figure (IPF), Kernel Average Misorientation (KAM), and Grain Boundary Density (GBD): (a1) IPF, (a2) KAM, and (a3) GBD of the homogenized sample H; (b1) IPF, (b2) KAM, and (b3) GBD of the sample H+MAF with the MAF process after homogenization; (c1) IPF, (c2) KAM, and (c3) GBD of the fully heat-treated sample H+A; (d1) IPF, (d2) KAM, and (d3) GBD of sample H+A+MAF with the MAF after full heat treatment; and (e1) IPF, (e2) KAM, and (e3) GBD of sample H+MAF+A with the MAF process between homogenization and aging processes.

Preprints (www.preprints.org) | NOT PEER-REVIEWED | Posted: 21 February 2022 doi:10.20944/preprints202202.0253.v1

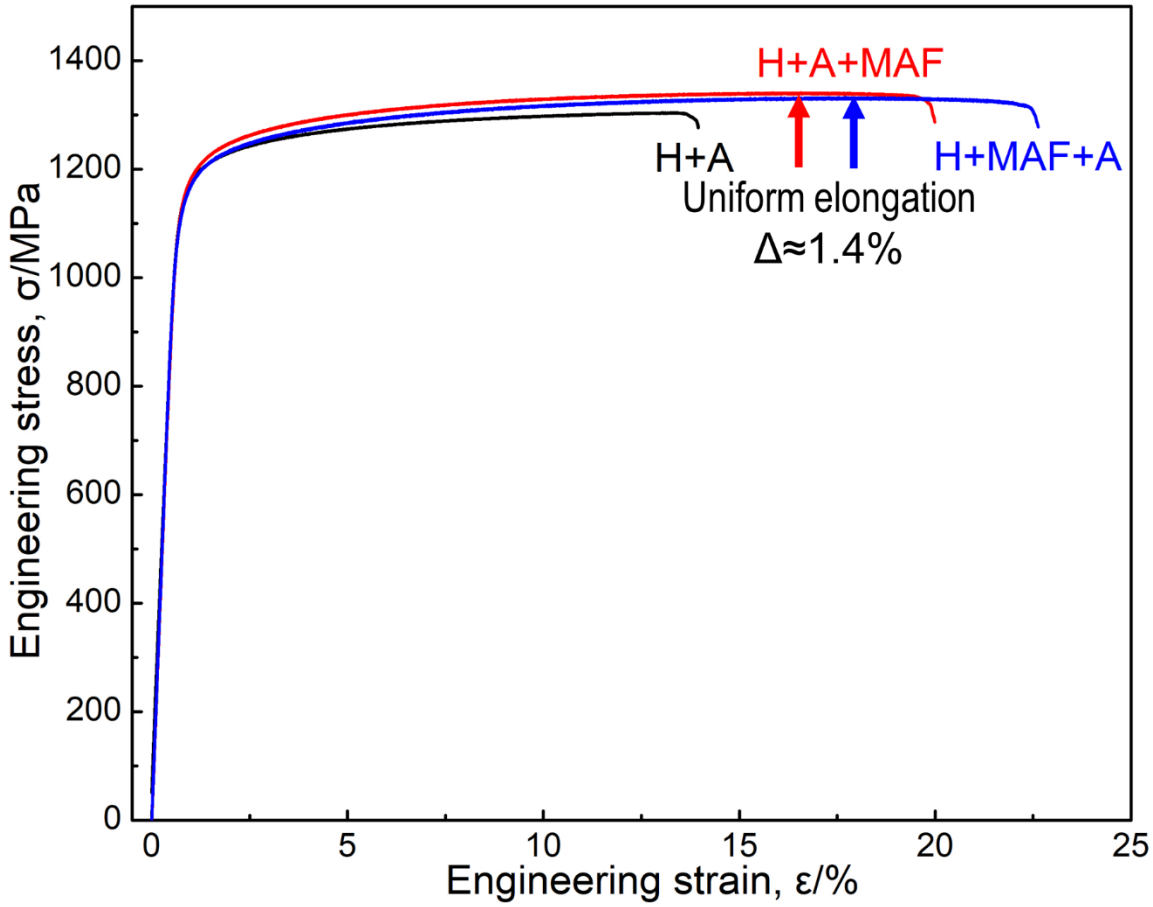

Figure 5. Stress-strain curves of the fully heat-treated sample H+A without MAF process, sample H+A+MAF with the MAF process after the full heat treatment, and sample H+MAF+A with the MAF process between homogenization and aging processes.

Preprints (www.preprints.org) | NOT PEER-REVIEWED | Posted: 21 February 2022 doi:10.20944/preprints202202.0253.v1

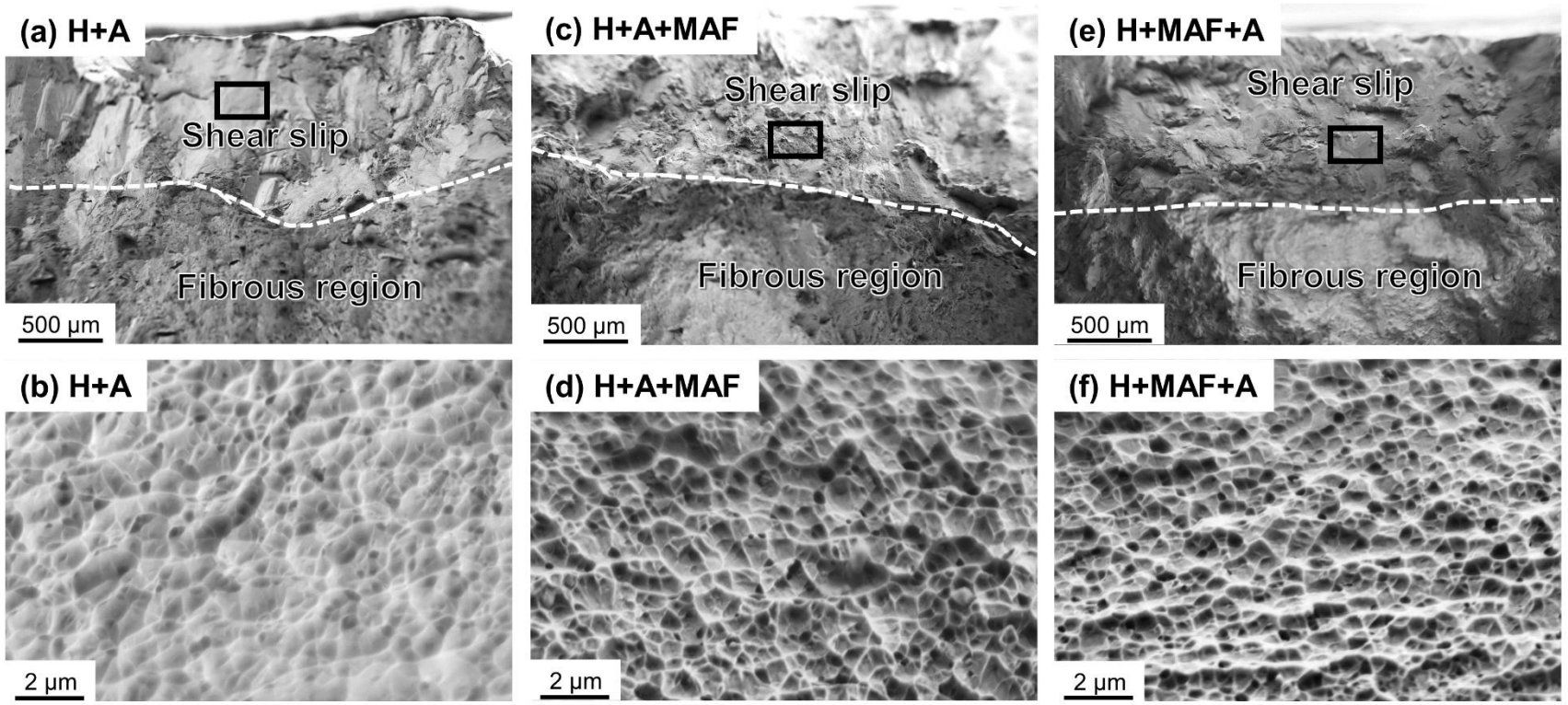

Figure 6. Fractography of (a) the fully heat-treated sample H+A without MAF process and (b) magnified area of sample H+A in the shear slip region; (c) sample H+A+MAF with the MAF process after full heat treatment and (d) magnified area of sample H+A+MAF in the shear slip region; and (e) sample H+MAF+A with the MAF process between the homogenization and aging processes and (f) magnified area of sample H+MAF+A in the shear slip region.